Phonon scattering in chemical-vapor-deposited diamond

J. E. Graebner, M. E. Reiss, and L. Seibles
AT&T Bell Laboratories, Murray Hill, New Jersey 07974

T. M. Hartnett, R. P. Miller, and C. J. Robinson
Raytheon Company, Lexington, Massachusetts 02173
(Received 14 March 1994)

The in-plane thermal conductivity $\kappa_{\parallel}$ has been measured over the temperature range 5–400 K for samples of chemical-vapor-deposited (CVD) diamond made by both the microwave and hot-filament processes. The samples span a range of defect level, grain size, and degree of thinning. Comparison with a model of heat transport suggests that $\kappa_{\parallel}$ is limited by scattering of phonons from point defects, extended defects of ~ 1.5 nm diameter, dislocations, grain boundaries, and microcracks, as well as by phonon-phonon scattering at high temperatures. The Callaway model of thermal conductivity is used to include the effects of normal three-phonon scattering processes. In the higher-conductivity samples, scattering of long-wavelength phonons is very weak even at grain boundaries, indicating relatively smooth boundaries. The value of $\kappa_{\parallel}=20\ \mathrm{W\,cm^{-1}\,K^{-1}}$ at room temperature for some of the microwave CVD samples is the highest reported to date for CVD diamond. Measurements of the anisotropy in conductivity obtained from the measured perpendicular conductivity $\kappa_{\perp}$ consistently show a higher conductivity along the (columnar) grains. The hot-filament-CVD sample measured exhibits a room-temperature conductivity approaching that of the best microwave-plasma samples, indicating that the thermal conductivity is determined more by the specific conditions of growth than by the type of CVD growth (microwave or hot filament).

INTRODUCTION

At temperatures above ~ 100 K, diamond has the highest thermal conductivity of any known substance.[1,2] This remarkable property arises from the strength of the carbon-carbon bond and the stiffness of the diamond lattice. Synthetic diamond made by the chemical-vapor-deposition (CVD) process[3] now provides polycrystalline diamond economically in the form of a plate, which is a convenient form for many applications. The quality of CVD diamond has increased rapidly in recent years and the thermal conductivity of the highest-quality plates now approaches that of the highest-quality single crystals. Our understanding of the defects limiting the thermal conductivity, however, is far from complete. The related question of the dependence of quality on preparation conditions also has no simple answer.

Early measurements[4–6] of thermal conductivity in thin CVD diamond films revealed values of $\kappa \approx 3-10$ W/cm K at room temperature with a positive temperature coefficient.[5] While remarkably high compared to that for other insulators, these values were considerably below the promise of 20–25 W/cm K characteristic of high-quality (type IIa) natural diamond.[1,2] More recent measurements[7,8] on thicker films of higher optical clarity yielded values around 17 W/cm K at room temperature with a negative temperature coefficient, much more similar to high-quality single crystals. The microstructure was soon shown to play a prominent role in determining the conductivity.[9–11] CVD diamond typically grows with long grains oriented perpendicular to the plane of the substrate, with the average grain diameter increasing with height above the substrate. Anisotropy in κ was observed,[10,11] with the conductivity $\kappa_{\perp}$ for heat flowing perpendicular to the plane of the substrate being typically 30% greater than for $\kappa_{\parallel}$ with heat flowing parallel to the plane of the substrate. With such a strong dependence on the grain orientation, it was further realized that a suitably defined local conductivity κ^{local} might be expected to be a function of the distance z from the substrate side of a thick film. Measurements[9,11] on a series of microwave-plasma (MP) CVD diamond films, all made under identical growth conditions and differing only in thickness (time of growth), showed indeed an overall κ which increased with film thickness, rather than remaining constant as would be expected for a homogeneous material. By subtracting the conductance of any sample from that of the next thicker sample, a local conductivity was deduced as a function of z. A large gradient was found for both $\kappa_{\parallel}^{\mathrm{local}}$ and $\kappa_{\perp}^{\mathrm{local}}$, increasing from 5 W/cm K near the substrate face to over 23 W/cm K near the top (growth) face of a sample that is at least 200 μm thick. $\kappa_{\perp}^{\mathrm{local}}$ increased more rapidly with z than did $\kappa_{\parallel}^{\mathrm{local}}$, accounting for the observed anisotropy in the overall conductivity. Measurements of κ over a large temperature range have been used[7,8] to determine the phonon scattering rate as a function of phonon wavelength in order to deduce the nature of the scattering entities. Wide-temperature-range measurements of the *local* conductivity have been used[8,12] to study the distribution of these entities within the material. Most of the above measurements were performed on some of the highest-quality samples available. CVD diamond generally occurs in a wide range of quality, as judged by optical clarity, thermal conductivity, in-

frared (ir) absorption, etc., but there is no clear association of high conductivity with any growth method or particular growth conditions. One study[7] has compared MP and hot-filament (HF) samples made in the same laboratory. The MP material was generally of higher conductivity than the HF, particularly in the 10–100 K temperature range. This was attributed to a greater abundance of unidentified extended defects in the HF material. We present here a study of a variety of MP samples of different grades and different degrees of thinning, as well as one unpolished HF sample. We find record high values for $\kappa_{\|}$ at room temperature for several of the MP samples and a conductivity for the HF sample that is nearly as high. Analysis of the temperature dependence of the conductivity suggests the presence of a number of defects, including microcracks.

EXPERIMENTAL DETAILS

The samples were prepared at Raytheon Company by MP and HF techniques under conditions somewhat similar to those described previously.[5,7] The samples were grown at substrate temperatures of 900–1000 °C with hydrogen and methane feed gases. The methane concentration was in the range 1–4 % by volume for the MP samples and 2% for the HF. For the latter sample (*E*1), 0.5% oxygen was added to the mixture. The growth rates are listed in Table I. The *An*, *Bn*, *Cn*, and *Dn* samples ($n=1$ or 2) are from four different runs in a microwave CVD system distributed over a period of approximately two years, during which time the growth parameters were fine tuned to produce higher-quality material as judged, for example, by the ir absorption. All microwave plasma samples were grown using high power densities (input power per substrate area >150 W/cm^2) and high chamber pressures (>100 Torr). Such plasma conditions generate high atomic hydrogen concentrations and allow high-quality diamond to be grown at relatively high rates from methane and hydrogen. The need for high atomic hydrogen concentration to grow high-quality diamond has been discussed previously.[13–15] In the case of hot-filament deposition, the quantity of atomic hydrogen available to the growing diamond surface is fixed by

TABLE I. Characteristics and fitted parameters for the eight samples labeled *A*1 through *E*1 grown in five runs by microwave-plasma (MP) or hot-filament (HF) chemical-vapor deposition. Five samples were thinned by mechanically polishing the top (growth) and bottom (substrate) surfaces. The average grain size is a simple average of the grain size measured on the top and bottom surfaces by the linear-intercept technique. The absorption α is obtained from the infrared spectra in Fig. 2; $\Delta\alpha$ is the approximate excess over the intrinsic absorption. The parameters *d*(fit), *P*, *E*, *F*, *S*, and *M* describe the fits of Eqs. (2) and (3) to the $\kappa_{\|}$ data in Figs. 6–8. *d*(fit) is the effective grain size or sample size, as detected by long-wavelength (low-temperature) phonons, while *P* and *E* are related to the concentration of point defects and extended defects (of diameter *F*), respectively. The concentration c_E of extended defects is obtained from *E* using Eq. (10). *S* is related to the concentration of dislocations, and $M<1.0$ allows for the presence of microcracks.

Quantity	*A*1	*A*2	*B*1	*B*2	*C*1	*D*1	*D*2	*E*1
Run number	RDH54	RDH54	RDH31	RDH31	RDD362	RDD383	RDD383	HFB69
Type	MP	MP	MP	MP	MP	MP	MP	HF
Growth rate (μm/h)	5.9	5.9	6.3	6.3	3	3	3	0.8
Removed, top (μm)	0	~130	0	~160	~130	~120	~120	0
Removed, bottom (μm)	0	~50	0	~50	~90	~17	~120	0
Final thickness (μm)	722	495	707	903	357	761	643	230
Width (cm)	0.298	0.289	0.293	0.300	0.602	0.353	0.350	0.295
Length (cm)	1.01	0.995	2.527	2.528	0.80	1.00	1.00	1.00
Raman FWHM top (cm^{-1})	3.4	2.9	4.0	2.1	1.6	1.7	1.5	2.4
Raman FWHM bot. (cm^{-1})	3.5	2.9	3.5	3.1	1.9	1.6	1.5	2.7
α(~1300 cm^{-1}) (cm^{-1})		0.2		1.7	0.25	0.05		0.7
$\Delta\alpha$(~2850 cm^{-1}) (cm^{-1})		0.5		4	0.3	0.1		1
Grain size, top (μm)	62	44	49	88	27	73	79	20
Grain size, bottom (μm)	15	11	~0	6	32	10	30	~0
Av. grain size *d*(obs) (μm)	38	28	25	47	30	42	55	10
$\kappa_{\|}$(298 K) (W/cm K)	13.3	17.2	8.7	10.2	20.0	20.2	20.0	15.7
$\kappa_{\perp}$(298 K) (W/cm K)	15.9	18.6	12.8	12.6	21.4	22.2	21.6	19.8
$\kappa_{\|}/\kappa_{\perp}$(298 K)	0.84	0.92	0.68	0.81	0.93	0.91	0.93	0.79
κ_{av}(298 K)	14.6	17.9	10.8	11.4	20.7	21.2	20.8	17.8
d(fit) (μm)	42	120	15.5	63	360	610	550	190
d(fit)/*d*(obs)	1.1	4.3	0.6	1.3	12	15	10	19
P (10^{-26} cm^3)	19	9.5	35	55	6.1	5.0	4.6	12.5
E (10^{-22} cm^3)	8.8	4.7	27	6.7	2.0	1.8	1.9	5.1
F (10^{-8} cm)	16	15	15	17	15	17	17	12
c_E (10^{16} cm^{-3})	4.2	3.4	19	2.3	1.4	0.6	0.6	14
$10^5 S$	16.8	6.7	43	5.8	3.8	4.1	4.7	3.4
M	0.96	0.93	0.95	1.0	0.95	0.90	0.88	0.95

the filament temperature (~2100 °C for sample $E1$) and area. Because of the lower concentrations of atomic hydrogen available, lower methane concentrations and short distances of the filament to the substrate are necessary to grow high-quality films. A high-quality diamond sample like $E1$ that was grown with 2% methane and 0.5% oxygen could also have been made without oxygen by using a lower methane concentration. The addition of oxygen has the same effect as lowering the methane concentration.[16] After the wafers were removed from the substrate and cut into samples, the samples (except for $A1$, $B1$, and $E1$) were polished to remove lower-quality material from the bottom (substrate) surface and the roughness of the top (growth) surface. More material was generally removed from the top surface (Table I) in order to produce a smooth surface over a relatively large area. Sample $D2$ is very similar in preparation to sample $D1$ except that ~100 μm more material was removed from the substrate side of $D2$.

Scanning electron microscopy was used to examine the morphology of the growth surface of three of the samples (Fig. 1) and to determine the average grain size (Table I). Sample $B1$ is of clearly inferior quality with poorly shaped growth facets and abundant secondary nucleation. To reveal grain boundaries on polished surfaces, the polished samples were etched briefly in a hot KNO_3 bath, which removes amorphous or graphitic carbon. It was noted that the grain boundaries of samples $A2$, $C1$, $D1$, and $D2$ were etched by the hot bath much more slowly than those of samples $B2$.

Fourier-transform infrared transmission measurements are shown in Fig. 2 for the polished samples (and for the unpolished sample $E1$). The spectra for all five samples are nearly identical in the 1700–2700 cm^{-1} region and show the shape characteristic of the intrinsic two-phonon absorption in diamond. The spectra were therefore normalized to the known[17] absorption coefficient of 12.31 cm^{-1} at a wave number of 2000 cm^{-1}. Absorption in the 900–1400 cm^{-1} region is defect-induced one-phonon absorption in diamond as discussed previously.[18–21] The interpretation of the defect-related absorption peaks for CVD diamond is very uncertain. However, if the feature at 1130 cm^{-1} in the spectrum of sample $B2$ is attributed to single substitutional nitrogen, a concentration of ~20 ppm is obtained. There is no evidence of nitrogen in the "A" or "B" forms often seen in the one-phonon region in natural diamond. Absorption due to C-H stretching vibrations of hydrogen impurities in these samples is present in the 2800–3000 cm^{-1} region. The higher quality of samples C and D is clearly seen by the low levels of these absorption features.

Raman scattering was performed with an illumination spot of ~1 mm diameter on the sample surface. Very little or no sign of a peak was observed near 1550 cm^{-1}, usually associated with amorphous-graphitic carbon (sp^2 bonding), while a very intense and narrow line was ob-

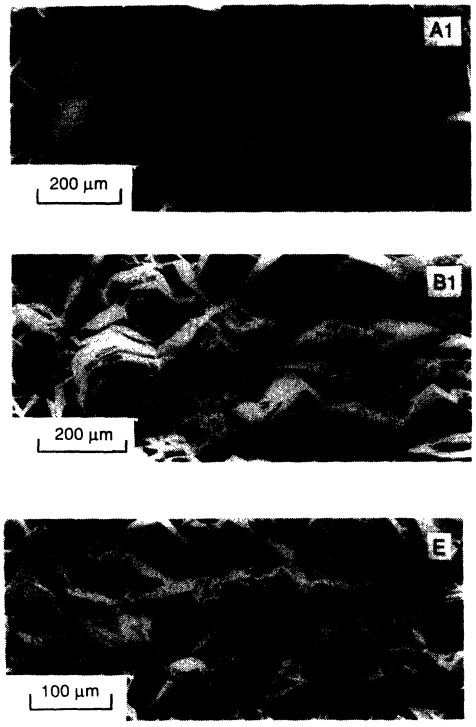

FIG. 1. Scanning-electron-microscope views of the top (growth) surfaces of microwave-plasma (MP) samples A1 and B1 and hot-filament (HF) sample E1. Note the relatively large and clean faces of samples A1 and E1, in contrast to the rough surfaces and secondary growth of sample B1. The smaller grain size of E1 is related to its thickness being ~$\frac{1}{3}$ that of A1 or B1.

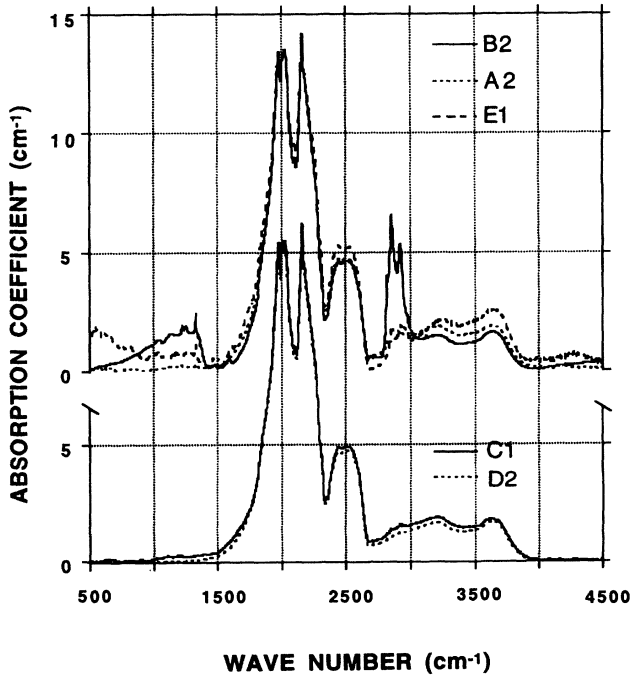

FIG. 2. Infrared spectra for five of the present samples. The absorption coefficient has been scaled to make all curves equal in the intrinsic absorption region at 2000 cm^{-1}.

served at 1332 cm^{-1}, characteristic of sp^3-bonded diamond. The full-width-at-half-maximum (FWHM) linewidths (Table I) indicate generally lower quality in samples $B1$ and $B2$, consistent with the infrared measurements. The extremely narrow lines in the C and D material were checked by extrapolating carefully to zero slit width. The average linewidth (1.6 ± 0.1 cm^{-1}) is the same as that for the best single-crystal diamond reported[22] and indicates the very high quality of these samples.

The parallel conductivity $\kappa_\parallel$ was measured with a technique[8] which is designed to avoid the considerable errors that can arise because of the exchange of thermal radiation between the sample and its surroundings or because of thermal transport along the electrical leads between sample and thermal ground. The technique is a variation of the standard heated-bar method. It consists of adding a second heater $H2$ near thermal ground, Fig. 3. The usual measurement of $\Delta T/\Delta x$ is taken with $H1$ energized. Then $H2$ is energized instead, and the temperature profile is examined for any gradient. If no heat is being lost from the sample by radiation or by conduction along the leads, zero gradient will be observed. If heat is being lost from the sample surfaces by radiation, a catenary temperature profile is expected,[23] Fig. 3(b). If heat is being lost through the $H1$ electrical leads, a linear profile is expected. In either case the loss can be modeled quantitatively and used to correct the gradient measured with only $H1$ energized. We have found that, for the diamond films we have measured, the small loss can be corrected for by simply subtracting the gradient measured with $H2$ powered from that with $H1$ powered. The samples are quite uniform in thickness and width, so that the estimated uncertainty in $\kappa_\parallel$, after the above corrections are made, is ~3%. We emphasize that without the use of $H2$ it is easy to be in error by 10–50% or more, especially at room temperature and above and with thinner samples or samples of lower conductivity.

A laser flash method[10,24] was used to measure the diffusitivity $D_\perp$ in the direction perpendicular to the plane of the film. The heat capacity[25] per unit volume C is then used to convert to thermal conductivity: $\kappa_\perp = CD_\perp$. An 8-ns pulse from a Nd:YAG laser is used[10] to deliver energy to one side of the sample which is coated on both sides with a 300-nm-thick layer of sputtered Ti. The arrival of the diffusive pulse at the far face is monitored by fast (100 MHz bandwidth) infrared detection of black-body radiation from the second Ti layer. Typical results and a fit to the one-dimensional diffusion equation are shown in Fig. 4. Several precautions must be taken with this technique. The simple solution to the one-dimensional diffusion equation[24] assumes an impulse of energy at the front face. In practice, this requires that the pulse length be no longer than ~1–2% of $t_{1/2}$, the time taken for the pulse to diffuse far enough through the sample that the temperature of the rear face rises to one-half its final value. Specifically, $t_{1/2} = 1.38Z^2/\pi^2 D_\perp$, where Z is the sample thickness. With the present pulse width, this exerts a lower limit on Z of ~25 μm, for dia-

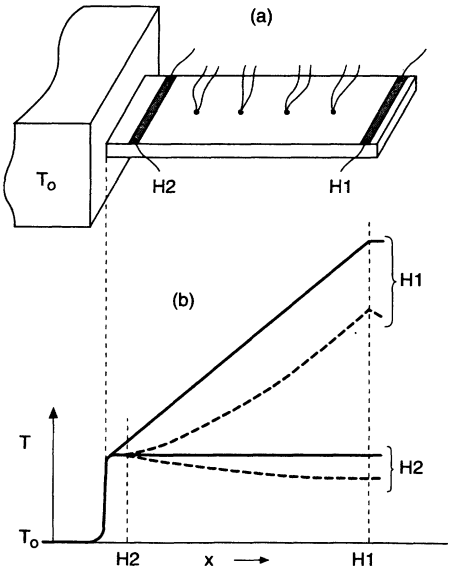

FIG. 3. (a) Schematic drawing of a sample mounted for measuring $\kappa_\parallel$. $H1$ and $H2$ are thin-film heaters deposited directly on the diamond sample, with four thermocouples (0.0025 cm diameter, Chromel-Constantan) attached with silver-filled epoxy. The sample is connected to a temperature-controlled (T_0) copper block with silver-filled epoxy. (b) Temperature distribution expected for electrical power applied to either $H1$ or $H2$, for two cases: zero radiation loss from the surface of the sample (solid straight lines) and severe radiation loss (dashed curves).

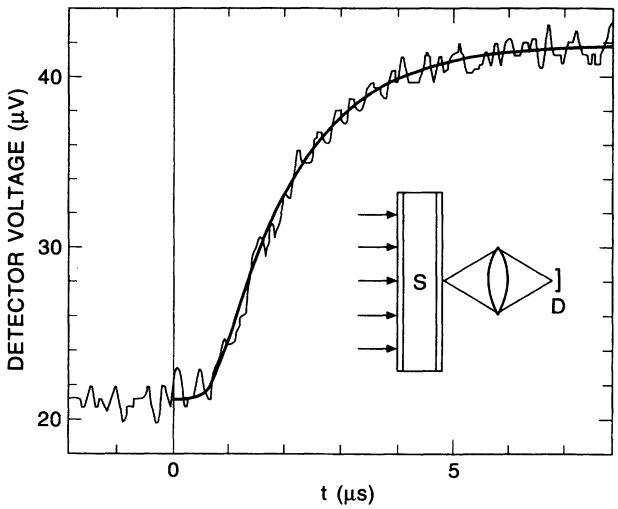

FIG. 4. Typical raw data for measuring $\kappa_\perp$. The output of the infrared detector is plotted vs time. The laser pulse occurs at the zero of time, and the data are averaged from 2000 laser pulses, occurring at a rate of 10 Hz. The total rise in temperature is approximately 0.3 °C. The sample thickness is 300 μm and the average temperature is 112 °C. The solid curve through the data is a least-squares fit of the solution of the one-dimensional diffusion equation, with a value of $D_\perp = 3 cm^2/sec$. The inset shows the sample S coated on both sides with a thin film of titanium. The laser pulse is incident from the left and a germanium ($f/1$) lens system focuses thermal radiation from the right side of the sample onto an infrared detector D.

mond films which for this thickness have typically $D_\perp \approx 3$ cm^2/sec. For thinner samples, the finite pulse width must be taken into account.

Another precaution must be observed when using the flash technique on a thick sample of material such as high-quality diamond in which the diffusivity is a strong function of the temperature. During the time of absorption of the optical pulse τ_0, the thermal energy diffuses into the sample to a depth $z_0 \approx (7D_\perp \tau_0)^{1/2}$. For an absorbed energy density of E (J/cm^2), the temperature in this surface layer will rise by an amount $(\Delta T)_0 \approx E/z_0 C$. As the pulse diffuses to a depth of $\sim 2z_0$, by conservation of energy the average temperature rise to a depth $2z_0$ will be reduced to $(\Delta T)_0/2$. In general, after the pulse diffuses to a depth nz_0, the average temperature rise there is $(\Delta T)_0/n$. A rough estimate of the average temperature of the material in which the heat is diffusing is then obtained by taking the spatial average, resulting in

$$(\Delta T)_{\rm av} = (\Delta T)_{\rm final} \ln(Z/z_0) ,$$

where $(\Delta T)_{\rm final}$ is the temperature rise in the long time limit, i.e., at least $\sim 5 \times t_{1/2}$ after the time of the pulse. That is, the measured diffusivity is characteristic of the material at a temperature $T_0 + (\Delta T)_{\rm av}$, where T_0 is the temperature of the sample just before the arrival of the laser pulse. Even for the relatively thick samples in the present study, if the final observed temperature rise is kept small (~ 0.3 K), the correction $(\Delta T)_{\rm av}$ can be kept reasonably small (~ 3–4 K), thus justifying the simple estimate presented here. Additionally, we have looked for but not found any difference in the measured diffusivity for heat traveling in either direction, i.e., from growth surface to substrate surface or the reverse.

The unpolished samples ($A1$, $B1$, and $E1$) with the as-grown rough top surface have an average valley-to-peak difference which is as much as 10% of the total thickness Z. We use half of this variation as effectively solid sample, i.e., we assume that the effective sample thickness is 5% less than measured to the top of the peaks. This is usually within $\sim 1\%$ of the average thickness deduced from measurements of the mass, length, and width of a sample, assuming a uniform sample thickness and a density equal to the density of bulk diamond. We have checked the latter assumption using Archimedes' principle at room temperature and found it to be accurate to the limit of the density measurement, $\sim 0.5\%$.

Signal averaging is used to improve the signal-to-noise ratio. Typical temperature resolution obtained is 0.005 °C. Thin samples (100 μm or less) require only several hundred laser pulses, while thick samples (~ 0.5 mm) require up to several thousand pulses. The typical scatter in the values for $D_\perp$ or $\kappa_\perp$ is $\pm 5\%$. The sensitivity of infrared thermometry varies as the cube of the absolute temperature, so that the scatter is somewhat worse than 5% at 300 K (especially for thick samples) and somewhat better at 400 K. The rapid temperature dependence of the sensitivity also restricts the present measurements of $\kappa_\perp$ to room temperature and above.

The steady-state technique and the laser flash technique were both applied to a plate of type-IIa natural diamond single crystal ($0.109 \times 5 \times 5$ mm^3), for which no anisotropy is expected. To within 1%, the two techniques gave the same result: 21.0 W cm^{-1} K^{-1} at room temperature, which is a typical value for type-IIa single crystals.

RESULTS AND ANALYSIS

The parallel and perpendicular conductivities for all samples in the temperature interval of 20–130 °C are shown in Fig. 5. $\kappa_\perp$ is consistently higher than $\kappa_\parallel$, and the conductivity of an unpolished sample ($A1$ or $B1$) is markedly lower than that of the polished sample of the same material ($A2$ or $B2$). Values of the room-temperature conductivities $\kappa_\parallel$ and $\kappa_\perp$ are listed in Table I. The measurements of $\kappa_\parallel$ were extended to liquid-helium temperatures, Figs. 6–8, to study the phonon scattering mechanisms. A peak in the data for $\kappa_\parallel$ occurs at a temperature which is lower the higher the room temperature conductivity. The temperature dependence at the lowest temperature is between T^2 and T^3 for most of the samples.

In order to understand the phonon scattering mechanisms responsible for thermal resistance in these samples, the conductivity can be calculated within the Debye phonon model with several contributions to the phonon scattering. The strengths of these scattering mechanisms can be varied individually to obtain a fit to a particular set of data. The conductivity of the phonons is usually expressed[26] as an integral over temperature T and phonon frequency ω:

$$\kappa = \frac{k_B}{2\pi^2 v}\left[\frac{k_B}{\hbar}\right]^3 T^3 \int_0^{\Theta/T} \frac{\tau(x) x^4 e^x dx}{(e^x - 1)^2} , \qquad (1)$$

where v is an averaged velocity of sound, k_B and $\hbar$ are Boltzmann's and Planck's constants, Θ is the Debye temperature, $x = \hbar\omega/k_B T$, and $\tau^{-1}(x)$ is the scattering rate at temperature T for a phonon of frequency ω. ($\omega = 2\pi v/\lambda$, where λ is the phonon wavelength.) One usually assumes that the scattering mechanisms are independent so that the scattering rates τ_i^{-1} are additive.

Recent studies[27–30] of synthetic diamond single crystals isotopically enriched in ^{12}C have shown a remarkably high sensitivity of thermal conductivity to the presence of a small amount (a few percent or less) of ^{13}C, particularly in the temperature region near the peak conductivity. In-

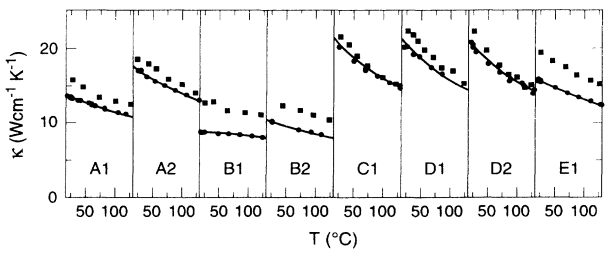

FIG. 5. Thermal conductivity measured parallel ($\kappa_\parallel$, circles) and perpendicular ($\kappa_\perp$, squares) to the plane of the sample for MP samples $A1$–$D2$ and for HF sample $E1$. Characteristics of the samples are given in Table I. The curves through the $\kappa_\parallel$ data are the same calculated curves as in Figs. 6–8 below.

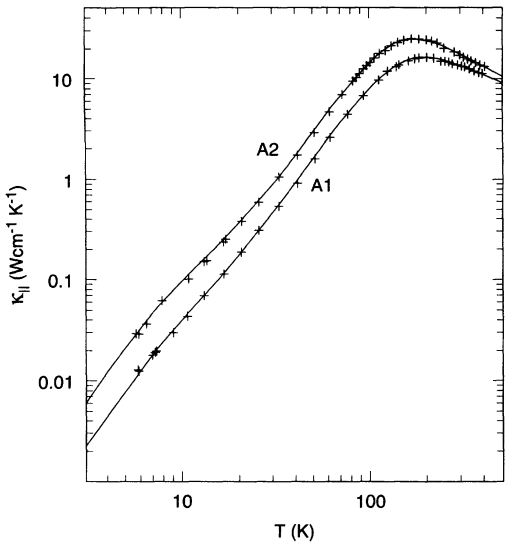

FIG. 6. Thermal conductivity $\kappa_{\|}$ vs T for MP samples $A1$ and $A2$. The solid curves through the data are fits using the model of thermal conductivity with parameters listed in Table I.

troducing 1.1% ^{13}C (the normal isotopic abundance) decreases κ(300 K) by $\sim$30% from its value in a nearly pure sample (0.07% ^{13}C). This effect, which is much larger than the $\sim$1–2% decrease expected from simple Rayleigh scattering from the ^{13}C point defects, has been attributed[29–34] to the presence of normal processes.

Phonon-phonon scattering is well known to play a dominant role in the conductivity of insulating crystals at high temperatures.[26] For $T \gtrsim \Theta/10$, enough large-wave-vector phonons are excited that the interaction of two phonons produces a third which has a significant probability of lying outside the first Brillouin zone, equivalent to a phonon traveling in the opposite direction after sub-

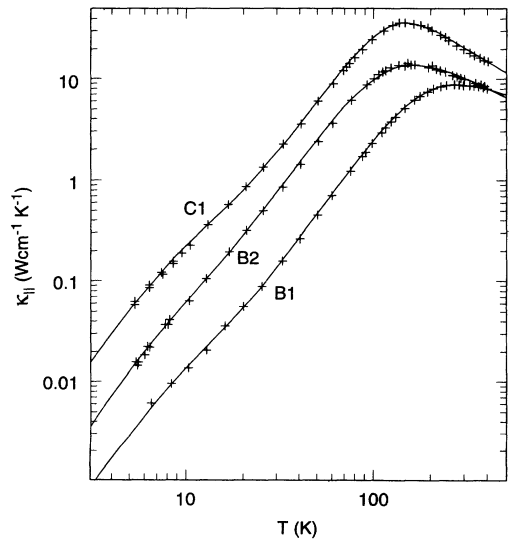

FIG. 7. Thermal conductivity $\kappa_{\|}$ for MP samples $B1$, $B2$, and $C1$. The solid curves through the data are fits using the model of thermal conductivity with parameters listed in Table I.

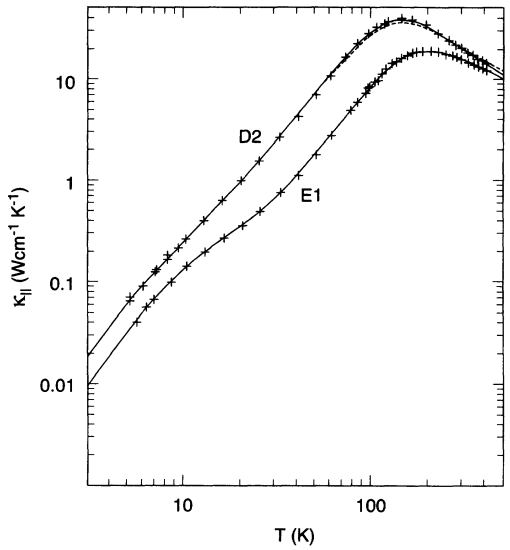

FIG. 8. Thermal conductivity $\kappa_{\|}$ vs T for MP sample $D2$ and HF sample $E1$. The data for sample $D1$ are not plotted but lie very close to those for sample $D2$. The curves through the data are fits using the model of thermal conductivity with scattering parameters listed in Table I. The dashed curve is a separate fit to the data of sample $D2$ assuming that no microcracks are present ($M=1.0$).

traction of a reciprocal lattice vector, thus introducing thermal resistance. Such umklapp scattering (U process) is thus distinguished from the scattering of smaller-wave-vector phonons, which does not involve a reciprocal lattice vector [normal (N) process] and which does not contribute directly to thermal resistance. However, the N processes do serve to exchange energy between low- and high-energy modes, which has the effect of increasing the thermal resistance if the dominant scattering mechanism is strongly frequency dependent (Rayleigh scattering, for example). This small extra resistance is usually negligible unless the total resistance is very small, i.e., unless one is near the peak conductivity in high-purity single crystals. Near the peak in diamond,[30] the conductivity of a sample with 1.1% ^{13}C is remarkably approximately three times smaller than that of a sample with 0.07% ^{13}C.

Because some of the present samples have a room-temperature conductivity within 10% of that of the very best single crystals of normal isotopic abundance, it was felt that the effects of N processes ought to be taken into account. The most widely used model which includes N processes is that due to Callaway,[35] in which the combined relaxation rate τ_C^{-1} is written as the sum of the normal (N) and resistive (R) rates: $\tau_C^{-1}=\tau_N^{-1}+\tau_R^{-1}$, where $\tau_R^{-1}=\sum_i \tau_i^{-1}$ is summed over all the resistive scattering mechanisms assumed to be present. The total conductivity can then be expressed as the sum $\kappa=\kappa_1+\kappa_2$, where we write

$$\kappa_1 = HT^3 \sum_{j=1}^{3} v_j^{-1} \int_0^{\Theta_j/T} \tau_C^j J_4(x)\,dx \tag{2}$$

and

$$\kappa_2 = HT^3 \sum_{j=1}^{3} \frac{v_j^{-1} \left\{ \int_0^{\Theta_j/T} (\tau_C^j/\tau_N^j) J_4(x)dx \right\}^2}{\int_0^{\Theta_j/T} (\tau_C^j/\tau_N^j\tau_R^j) J_4(x)dx} , \quad (3)$$

with $\Theta_j = (6\pi^2/V_0)^{1/3}\hbar v_j/k_B$ as the Debye temperature associated with mode j. V_0 is the atomic volume (5.68×10^{-24} cm^3), $H = k_B^4/6\pi^2\hbar^3$, $1/\tau_C^j = 1/\tau_N + 1/\tau_R^j$, and $J_4 = x^4e^x(e^x-1)^{-2}$. This form follows Refs. 29 and 30 in separating the contributions of longitudinal and transverse modes. We point out that this formulation of the Callaway model does not account for interactions between phonons of different modes.[34]

The scattering mechanisms assumed for the present analysis have been written in terms of their velocity and wavelength dependence explicitly to facilitate the separation by mode.[29,30] (We omit j superscripts for clarity.) This approach avoids using a velocity which is averaged over the modes, an average which should in principle be different for each scattering mechanism.

(1) For umklapp scattering, we use a form which was found[8] to account well for the temperature dependence of the conductivity of single-crystal diamond over a wide temperature range:

$$\tau_u^{-1} = BvT\lambda^{-2}\exp(-C/T) . \quad (4)$$

Equation (4) has also been used recently on isotopically purified diamond single crystals,[28-30] with the most recent and perhaps most accurate determination (including N processes) of the constants being[30] $B = 1.5\times10^{-12}$ cm/K and $C = 670$ K.

(2) The expression for N processes has been taken to be

$$\tau_N^{-1} = AvT^3/\lambda , \quad (5)$$

a form used[36] on data of LiF with varying concentration of ^{6}Li. This is also the form used recently in Ref. 30, where a value of $A = 7.2\times10^{-11}$ K^{-3} was determined for diamond. Using the values of A, B, and C from Ref. 30, we have obtained similar agreement with the single-crystal diamond data included in Ref. 30, and we use those values without modification in the present analysis. Thus, we assume that the intrinsic scattering in diamond is well described by the values of A, B, and C of Ref. 30 and we add the extrinsic scattering mechanisms listed below to fit our data for CVD diamond.

(3) Point-defect scattering from isolated atoms of different mass (either different isotopes or different elements) gives rise to the familiar Rayleigh ω^4 dependence

$$\tau_P^{-1} = Pv/\lambda^4 . \quad (6)$$

P is related[26,37] to the concentration c_P of point defects with mass defect Δm by

$$P = 4\pi^3 c_P V_0 \left(\frac{\Delta m}{m} + 2\gamma\alpha \right)^2 , \quad (7)$$

where m is the mass of the host atom, γ is the Grüneisen constant for diamond, taken[38] to be 1.1, and α is the fractional volume difference between impurity and host atoms. For a single substitutional nitrogen atom in diamond,[39] $\alpha = 0.15$, while[29] for ^{13}C, $\alpha = 0.0005$. For vacancies,[40] the quantity in brackets in Eq. (7) takes on the value 3. Thus, a ^{13}C impurity scatters 35 times *less* than a single N impurity, while a single vacancy scatters 35 times *more* than a N impurity.

(4) For an extended defect, such as a cluster of foreign or disordered atoms, one also expects Rayleigh scattering for wavelengths that are large compared to the size of the defect. At higher frequencies, interference effects become important and eventually the scattering cross section becomes independent of frequency, i.e., the geometric limit is reached, for which the scattering cross section is $\sigma_E = \pi F^2/4$ for a spherical object of diameter F. The Rayleigh scattering varies as ω^4 and the crossover occurs at $\lambda_c = 2\pi F$. (For objects with symmetry lower than spherical, Rayleigh scattering follows a lower power of ω.) A simplified version[41] of the theoretical models for spherical objects can be used for such scattering:

$$\tau_E^{-1} = \begin{cases} Ev\lambda^{-4} & \text{for } \lambda > 2\pi F , \quad (8) \\ Ev\lambda_c^{-4} = c_E v\sigma_E & \text{for } \lambda < 2\pi F , \quad (9) \end{cases}$$

where the concentration of extended defects is c_E and the second equality in Eq. (9) arises by the definition of a cross section. Thus,

$$E = 4\pi^5 c_E F^6 . \quad (10)$$

More complicated expressions[42] for τ_E^{-1} can be used for a more accurate representation of the theoretical cross section.

It has been suggested independently by a number of authors[7,8,43,44] that scattering from extended defects can account for a relative dip in the measured conductivity of CVD diamond in the vicinity of 10–100 K. Resonant scattering[7,8,26,45] from a defect with an appropriate energy-level splitting could also produce such a broad dip, but in practice this is indistinguishable from Rayleigh scattering by extended defects. We will emphasize extended-defect scattering in this report, being aware that an alternative description in terms of resonance scattering is equally valid until independent microscopic evidence of the defects is available.

(5) Scattering from the strain field surrounding a dislocation[26] has been shown to vary as v/λ, with maximum scattering strength for the phonon wave vector oriented perpendicular to the axis of the dislocation. For an array of dislocations with random orientations, one has

$$\tau_S^{-1} = Sv\lambda^{-1} . \quad (11)$$

An upper limit on the density of dislocations per unit area N_S is given approximately by

$$N_S \ (\text{cm}^{-2}) \sim \gamma^{-2}b^{-2}S \sim 4\times10^{15}S , \quad (12)$$

where b is the Burgers vector of the dislocation. Vibration of the dislocation can increase its scattering strength,[26] effectively decreasing the proportionality constant in Eq. (12) by as much as 2–3 orders of magnitude. Thermal conductivity therefore does not yield a reliable value of the dislocation density.

(6) Boundary scattering is usually important at the

lowest temperatures where other scattering mechanisms are generally weak. If the scattering at the surface of the sample is diffuse,

$$\tau_B^{-1}=v/\alpha d \ , \tag{13}$$

where d is the sample size in a direction perpendicular to the direction of heat flow, and α is a constant of order unity which depends on the geometry of the sample.[46] For a circular cylinder of diameter d, $\alpha=1.0$, while for a cylinder of square cross section with side d, $\alpha=1.12$. For a plate,[47] α varies slowly with the geometric mean of thickness Z and width W. For a typical CVD diamond plate with $d=Z=0.3$ mm and $W=5$ mm, $\alpha\approx 3$. This expression for τ_B^{-1} successfully describes heat flow along the axis of long, thin, single-crystal samples[26] with surfaces that are rough on the scale of the phonon wavelength. For such surfaces, the direction of travel of a phonon after collision with the surface is unrelated to its direction before collision (diffuse scattering). For surfaces that are smooth on such a scale, specular (mirrorlike) reflection at the surface can decrease the effect of boundary scattering by making the sample appear larger than it actually is.[46,48,49] In that case, Eq. (13) should be rewritten as

$$\tau_B^{-1}=\left[\frac{1-p}{1+p}\right]v/\alpha d \ , \tag{14}$$

where p is the probability of specular reflection ($0\le p\le 1$). For measurements spanning a wide temperature range and therefore a wide range of wavelengths, reflections of the dominant phonons can be specular at low temperatures but diffuse at high temperatures. A wavelength-dependent probability $p[\omega]$ can be defined as[48,50]

$$p[\omega]=\exp[-(2\eta_{\rm eff}\omega/v)^2] \ , \tag{15}$$

where $\eta_{\rm eff}$ is the rms surface roughness. In this picture, scattering is diffuse for $\lambda\ll 4\pi\eta_{\rm eff}$ and specular for $\lambda\gg 4\pi\eta_{\rm eff}$.

The effect of a short sample can be approximated[49,51,52] by adding a term v/L to τ_B^{-1} in Eq. (14), where L is the sample length (in the direction of heat flow).

In most analyses of CVD diamond thermal conductivity reported to date, the simple expression in Eq. (13) has been used, with d being an average grain size. A value of $\alpha=1.12$ has usually been adopted, completely without justification. [Using this approach, it was suggested quite early[53] that the very small grain size ($\lesssim 10\,\mu$m) of thin polycrystalline diamond films can have an adverse effect on κ even at room temperature.] For $\kappa_\parallel$ in polycrystalline diamond with heat flowing *perpendicularly* to columnar grains, however, Eq. (13) must be modified. While we know of no rigorous treatment of the effective mean free path due to boundary scattering in a polycrystalline material with columnar grains, perhaps the most appropriate value of the effective grain size d is obtained by drawing a straight line across a photomicrograph of the grain structure and measuring the average distance between successive boundary crossings (the linear intercept method) and setting $\alpha=1.0$. To model boundary scattering accurately across columnar grains would require the analogs of Eqs. (14) and (15) for a polycrystalline material. In fact, a reasonably good fit[44,54] to early data[5] was obtained by simply using Eqs. (14) and (15) directly. [Equations (14) and (15) can produce an upwardly concave temperature dependence but by themselves cannot account for the $\sim T^3$ dependence at the lowest temperatures, as is apparent from the fit in Ref. 44.) We expect that a proper treatment of grain-boundary scattering will yield expressions very similar to Eqs. (14) and (15) but with $p[\omega]$ interpreted as the probability of *transmission* of a phonon *through* a grain boundary.

(7) At the highest frequencies and temperatures, some of the above scattering mechanisms lead to unphysically small mean free paths. To avoid this, one can require that

$$\tau_R[\omega]=l_{\rm min}/v+\left[\sum_i(\tau_R^i)^{-1}\right]^{-1} \ , \tag{16}$$

where $l_{\rm min}$ is a minimum mean free path and the second term on the right includes all of the above resistive scattering mechanisms. $l_{\rm min}$ has been modeled as either an interatomic dimension[8] or a half wavelength,[29] and typically becomes significant only at temperatures well above the present temperature range. For the fits to the present data, the half-wavelength approach has been used.

(8) The role of microcracks between grains has not been explored previously. If present, they would have a very deleterious effect on $\kappa_\parallel$, as the probability of transmission across the boundary would drop to zero even if the thickness of the crack were only of interatomic dimensions (~ 1 nm). One might expect the lateral extent of any microcrack between grains to be on the order of the grain size, i.e., at least a few micrometers. Since this is much larger than the wavelength of the heat-carrying phonons even at our lowest temperatures, simple geometric scattering of phonons by the microcracks would be expected throughout our temperature range. That is, the effect of microcracks would be to make the heat path somewhat more tortuous and longer than indicated by the macroscopic sample geometry. To allow for the possibility of such scattering, the conductivity calculated with Eq. (1) or Eqs. (2) and (3) can be multiplied by a temperature-independent constant $M\le 1.0$.

It is seen that, within this model, umklapp scattering is the only source of a negative temperature coefficient. This is because the integrand in Eq. (1) is always positive, so that the only way[55] to have the integral decrease with increasing T is to have an explicit and positive dependence of τ^{-1} on temperature, which is provided by τ_u.

Using the above model, we have adjusted the parameters P, E, F, S, d, and M to obtain a best visual fit to the data. The final adjustments of each parameter were done at the 3–10% level. The results are shown in Figs. 6–8, with the fitted parameters listed in Table I. Since the different parameters tend to dominate the conductivity in different temperature regions, the fits are more unique than might be expected with this many parame-

ters. Some insight into the roles of the various scattering mechanisms can be gained by examining the conductivity calculated with successively more scattering factors (Fig. 9). With only boundary and umklapp scattering, and a half-wavelength lower limit on the mean free path, one finds a T^3d temperature dependence at temperatures well below the peak. Umklapp scattering is equal to boundary scattering at the temperature of the maximum and dominates at higher temperatures. Point-defect scattering at the level needed to fit the data of sample $B1$ is increasingly important from ~ 60 K up to the highest temperatures, whereas the scattering from extended defects of 1.6 nm diameter is important only for $7 \lesssim T \lesssim 200$ K and is used to fit the dip in the data centered at $T \sim 30$ K. Scattering from dislocations tends toward a T^2 conductivity. The effect of microcracks is to reduce the entire $\kappa_{\|}(T)$ curve by a constant amount—10% in the case of sample $B1$. Without such an effect, we are not able to obtain a good fit in the temperature range of 150–400 K. Bringing the model conductivity down to the data in this temperature region by increasing the amount of point-defect, extended-defect, or dislocation scattering *without* microcracks invariably results in too small a slope and a poor fit. This is illustrated in Fig. 8 for sample $D2$, where the best fit without microcracks is shown by the dashed line. The effects of microcracks are most noticeable for high-conductivity samples ($C1$, $D1$, and $D2$). The values of M for the other samples are less well determined. We find that if the standard model [Eq. (1)] rather than the Callaway model is used, the microcrack corrections needed to fit the data are more serious than reported here, i.e., the deviation of M from 1.0 would be approximately twice what is indicated in Table I.

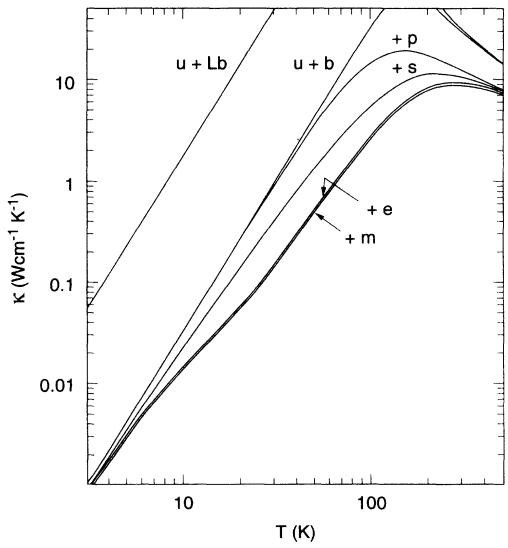

FIG. 9. Thermal conductivity of diamond calculated with Eqs. (2) and (3). The uppermost curve is obtained using only boundary scattering (large sample, $d=1$ mm) and umklapp scattering. The curve labeled $u+b$ is the same but with $d=15.5$ μm, as found for sample $B1$. The remaining curves are calculated with additional scattering by point defects (p), dislocations (s), extended defects (e), and microcracks (m), respectively, with parameters (Table I) adjusted to fit the data of sample $B1$ in Fig. 7.

We note that the values of M in Table I imply, for samples $C1$, $D1$, and $D2$, an average conductivity for crack-free samples of $\kappa_{\|}(298\ \text{K})/M = 21$–$23\ \text{W cm}^{-1}\text{K}^{-1}$, i.e., typical of type-IIa single crystals and within 10% of the conductivity of the very best type-IIa single crystals reported so far[29,38] (24–25 $\text{W cm}^{-1}\text{K}^{-1}$).

Figure 9 shows that, within this model, the room-temperature thermal resistance of sample $B1$ is dominated by point defects, while extended defects, dislocations, and microcracks play a lesser role; diffuse scattering at grain boundaries is insignificant at room temperature. A somewhat more quantitative estimate of the importance of each scattering mechanism can be obtained by repeating the calculation of $\kappa(T)$ with only one of the scattering mechanisms turned off at a time. Such calculations show that the thermal resistance introduced by each of the scattering mechanisms at room temperature, as a fraction of the total resistance, is as follows: boundaries, $\sim 0.2\%$; point defects, $\sim 49\%$; extended defects, $\sim 12\%$; dislocations, $\sim 13\%$; and microcracks, 5%.

The model provides a reasonably good fit to the data in Figs. 6–8 despite the fact that one expects the samples, especially the unpolished ones, to have a considerable gradient in grain size, defect density, and, therefore, conductivity as a function of height above the substrate, as found previously for other samples[9,11,12] of CVD diamond. The fitted parameters must be thought of as averages over the thickness of each specimen.

Scattering from irregular grain boundaries can dominate the thermal resistance at low temperatures, where other scattering mechanisms are weak. The use of scattering from rough grain boundaries (diffuse scattering) all the way down to helium temperatures produces an improved fit to the data by providing a slight downturn (toward a T^3 variation) at the lowest temperatures for the relatively poor conductors, samples $B1$ and $B2$. The grain size d(fit) needed for the fit is very close to the average grain size d(obs) measured from micrographs (Table I). For samples of overall higher conductivity, however, the grain size needed to fit the low-temperature data is considerably larger than the observed grain size: up to $4\times d$(obs) for $A2$ and 10–$20\times d$(obs) for samples $C1$, $D1$, $D2$, and $E1$. For the last four samples, in fact, the "grain size" needed to fit the low-temperature data is approximately the sample thickness, indicating that, at least for the long-wavelength phonons dominant at 5–10 K ($\lambda \sim 200$–400 nm), scattering at grain boundaries in these samples is insignificant. That is, the boundaries are smooth on the length scale of these phonons and the probability p for transmission through the boundary is close to unity. Recent measurements[56] of $\kappa_{\|}$ in CVD diamond down to $T=0.15$ K also indicate weak scattering of long-wavelength phonons at grain boundaries. Presumably at higher temperatures a boundary roughness [η_{eff} in Eq. (15)] would scatter the shorter wavelengths dominant at those temperatures, and if there were no other scattering mechanisms one could apply Eq. (15) to determine a value for η_{eff}, using $\alpha d = d$(obs). Because of generally heavy scattering by defects and dislocations in

the temperature range where one might expect a crossover from full transmission to diffuse scattering to occur ($\sim$10–100 K), it is very difficult to arrive at a unique value for η_{eff}. Therefore we have chosen to use for boundary scattering only Eq. (13) [with $\alpha=1.0$ and $d=d(\text{fit})$] at the risk of including a small amount of high-temperature grain-boundary scattering in P, E, and S for some of the samples. (Alternatively, the dip could be fitted by using Eqs. (14) and (15) [with a very small grain size, $d(\text{fit})\approx d(\text{obs})/10$], and the $\sim T^3$ dependence at the lowest temperature could be fitted by simultaneously using Eq. (13) with a mean free path approximately equal to the sample thickness.) The approach we have chosen has the benefit of reducing the number of adjustable parameters.

Because of the remarkably long mean free paths in some samples at low temperatures [$d(\text{fit})/d(\text{obs})\approx 10-20$], it is clear that extending measurements of κ to liquid-helium temperatures is not a reliable way to determine grain size, but combined with independent measurements of grain size it provides a good indication of the quality of the grain boundaries.

DISCUSSION

The room-temperature anisotropy (Fig. 5 and Table I) shows a strong dependence on the removal of material from the top and bottom surfaces by mechanical polishing. The ratio $\kappa_\parallel/\kappa_\perp$ is generally closer to unity (less anisotropy) for polished samples $A2$, $B2$, and $D2$. This anisotropy in κ is comparable to previous observations[11] using other (MP, thinner) samples, for which the anisotropy was shown to be due to a steeper gradient with respect to z for $\kappa_\perp$ than for $\kappa_\parallel$, for the first ~ 100 μm on the substrate side of an unpolished sample. The slightly greater anisotropy for the (unpolished) HF sample ($E1$) may be due to its thinness and the resulting greater fraction of its thickness occupied by the fine-grained low-conductivity material on the substrate side. The anisotropy is lowest ($\kappa_\parallel/\kappa_\perp>0.09$) for thick, polished, high-conductivity samples $C1$, $D1$, and $D2$.

Anisotropy of the thermal conductivity in a cubic lattice is prohibited by symmetry arguments.[47] However, the presence of boundaries lowers the symmetry and can yield anisotropy in the boundary-limited regime due to phonon focusing, which arises if the phase velocity and group velocity are not collinear. This has been observed[47] in single-crystal Si where $\kappa_{\langle 100\rangle}=\beta\kappa_{\langle 110\rangle}$ with $\beta_{\text{obs}}=1.38$, close to the (average) calculated value of $\beta=1.43$. Calculations[47] for diamond predict $\beta=1.40$. This has also been observed in diamond single crystals at low temperature.[57] However, this effect cannot explain the anisotropy in CVD diamond, as the axis of the grains is predominantly $\langle 110\rangle$. The observation that $\kappa_\perp>\kappa_\parallel$ would require $\beta<1.0$. In addition, the room-temperature conductivity is predominantly defect limited, rather than boundary limited, which would imply a value of β much closer to 1.0. We conclude that the anisotropy in CVD diamond is not due to the intrinsic elastic anisotropy of the diamond lattice.

Another potential source of anisotropy is a preferred orientation for nonspherical defects, such as dislocations. If the defects are aligned, e.g., dislocations aligned along the grain axis which is often a $\langle 110\rangle$ direction, one would expect $\kappa_\parallel<\kappa_\perp$, as observed. The correlation of a high value of S and a large anisotropy $\kappa_\parallel=0.68\kappa_\perp$ for sample $B1$ would lend support to such a situation. However, as noted above, dislocation scattering produces only $\sim$13% of the total thermal resistance in sample $B1$, less than half the amount required to explain the anisotropy.

Yet another potential source of anisotropy is a preferred location of defects at or near grain boundaries. The long, thin grains would provide a smaller average cross section of defective material when viewed along the grains ($\kappa_\perp$) than when viewed across them ($\kappa_\parallel$). That is, for $\kappa_\perp$, the defective regions near grain boundaries would be less effective in producing thermal resistance because they are in *parallel* with the (lower-resistance) grain bodies, whereas for $\kappa_\parallel$ they are in *series*. Such concentration of defects near grain boundaries is suggested by transmission electron microscopy work[58–60] and also by very recent cathodoluminescence studies[61] on similar samples made at Raytheon. The very low anisotropy of samples $C1$, $D1$, and $D2$ and the observed tendency for these samples to be chemically etched at grain boundaries less rapidly than for the lower-conductivity samples is consistent with thermal-resistance defects being located near grain boundaries.

The absolute value of the strength P of point-defect scattering demonstrates the high quality of the better samples, $C1$, $D1$, and $D2$. For these samples, P is comparable with the value of 5.3×10^{-26} cm^3 which is expected on the basis of Eq. (7) for 1.1% ^{13}C distributed on random lattice sites. Thus one might expect an increase in conductivity if these samples had been grown with isotopically purified gas. Such an isotope effect has recently been observed[62] in CVD diamond.

The strength S of scattering from dislocations suggests a dislocation density $N_S\sim10^{11}-10^{12}$ cm^{-2} for fixed dislocations or 10^8-10^{10} cm^{-2} if the dislocations are free to vibrate. This relatively large uncertainty could be resolved by an independent correlation of S with a known N_S in diamond. The density of dislocations in the present samples has not been determined by independent means.

The strength P of the point-defect scattering, the concentration c_E of extended defects, and the strength S of dislocation scattering are all correlated inversely with the average room-temperature conductivity of the MP samples (Table I). The high values of P in samples $B1$ and $B2$ are undoubtedly related to the high level of defects apparent in the ir spectrum for $B2$ (Fig. 2), particularly the hydrogen-related defects. (The low level ($\sim$20 ppm) of nitrogen possibly occurring in sample $B2$ is approximately two orders of magnitude too low to account for the observed point-defect scattering.) Compared with the MP samples, the HF sample is not unusual in either its point-defect or dislocation scattering but does show an especially large concentration of extended defects, with somewhat smaller diameters (1.2 nm) than is typical in MP samples (1.5–1.7 nm). This agrees with previous work[7] in which HF samples exhibited a stronger dip than

MP samples. It was proposed that metal impurities from the filament might be associated with the extended defects. The quality of HF material made at Raytheon has apparently improved over the last two years, as sample $E1$ exhibits a concentration of 1.4×10^{17} cm^{-3} extended defects of diameter 1.2 nm, which is $\sim$35 times lower than the concentration of 5×10^{18} cm^{-3} of 0.5-nm-diameter defects reported previously.[7] This may be due to better control over contamination of the diamond by the incorporation of filament atoms. We note that the scattering of phonons by extended defects is much weaker at room temperature than at low temperature, allowing the (unpolished) HF sample to have $\kappa_{\|}(298\ \mathrm{K})=15.7$ W cm^{-1} K^{-1}; this may be compared with 13.4 W/cm K for the previous best HF sample reported.[7] We emphasize that *all* samples discussed here (MP as well as HF) display a broad dip centered in the vicinity of 20–30 K. Previously reported[7] conductivity data of MP samples appeared not to display this feature, perhaps because the data did not extend low enough in temperature to resolve the dip which, in MP samples, tends to occur at somewhat lower temperatures than in HF samples. We further note that, for most samples, the data could be fit better if a range of diameters F were assumed. While one might expect to find such a distribution in a real sample, we have decided to retain a minimum number of parameters by assuming a fixed diameter for the extended defects.

It is interesting to correlate the average room-temperature conductivity (Table I) with the surface morphology of the unpolished samples (Fig. 1), the Raman linewidth (Table I), the ir absorption (Fig. 2 and Table I), and the growth rate (Table I). The lowest-conductivity sample ($B1$) is also the one prepared at the highest growth rate; it shows a higher degree of secondary nucleation, as well as the broadest Raman linewidth and highest defect-related absorption. The inverse correlation of conductivity with growth rate has been observed before,[63] but not for such high-quality films or such high overall growth rates. The *unpolished* sample with the highest conductivity is the HF sample ($E1$), which has clean facets, significantly less secondary growth, and the narrowest Raman linewidth of the three unpolished samples. We note the HF sample ($E1$), with an average grain size of 10 μm, has a higher conductivity than $A1$, $A2$, $B1$, or $B2$, all of which have grain sizes 2–5 times larger than that of $E1$. The high ratio of $d(\mathrm{fit})/d(\mathrm{obs})=22$ suggests that the grain boundaries in sample $E1$ have significantly fewer large defects than in the A or B material. The record-high values of $\kappa_{\|}(298\ \mathrm{K})=20$ W cm^{-1} K^{-1} for the most recently grown samples ($C1$, $D1$, and $D2$) and $\kappa_{\|}(143\ \mathrm{K})=42$ W cm^{-1} K^{-1} for samples $D1$ and $D2$ are correlated with the lowest growth rates (for the MP samples), the lowest defect-related infrared absorption, and the remarkably narrow Raman linewidths, and may also be due to particularly clean grain boundaries.

CONCLUSION

Measurements of thermal conductivity over a wide temperature range are reported for a variety of samples of CVD diamond spanning a range of defect level, grain size, and degree of thinning. Comparison with a model of thermal conduction indicates that, below $\sim$200 K, $\kappa_{\|}$ is dominated by scattering of phonons from point defects, extended defects, dislocations, and grain boundaries. At higher temperatures, umklapp scattering becomes dominant. It is shown that the fit to the model is improved significantly if microcracks are assumed to exist. Measurements of the anisotropy in κ suggest that the defects are located at or near grain boundaries. These results are consistent with previous measurements on other samples of high-quality CVD diamond. The room-temperature value of $\kappa_{\|}=20$ W cm^{-1} K^{-1} for several polished MP samples is higher than any previously reported for CVD diamond to our knowledge. A sample made by hot-filament CVD was found to exhibit a room-temperature conductivity nearly as high as the best MP samples, suggesting that the thermal conductivity is determined more by the specific conditions of growth than by the type of process used, i.e., hot-filament or microwave CVD. The average room-temperature conductivity is related inversely to the growth rate, the Raman FWHM, and the defect-related ir absorption.

ACKNOWLEDGMENTS

We would like to thank S. Jin, R. Berman, P. G. Klemens, and L. Wei for many useful discussions and G. W. Kammlott for electron microscopy.

[1] R. Berman, in *The Properties of Diamond,* edited by J. E. Field (Academic, London, 1979), Chap. 1.

[2] J. Wilks and E. Wilks, *Properties and Applications of Diamond* (Butterworth-Heinemann, Oxford, 1991).

[3] J. C. Angus, Y. Wang, and M. A. Sunkara, Annu. Rev. Mater. Sci. **21**, 221 (1991).

[4] A. Ono, T. Baba, H. Funamoto, and A. Nishkawa, Jpn. J. Appl. Phys. **25**, L808 (1986).

[5] D. T. Morelli, C. P. Beetz, and T. A. Perry, J. Appl. Phys. **64**, 3063 (1988).

[6] J. E. Graebner, J. A. Mucha, L. Seibles, and G. W. Kammlott, J. Appl. Phys. **71**, 3143 (1992).

[7] D. T. Morelli, T. M. Hartnett, and C. J. Robinson, Appl. Phys. Lett. **59**, 2112 (1991).

[8] J. E. Graebner and J. A. Herb, Diamond Films Technol. **1**, 155 (1992).

[9] J. E. Graebner, S. Jin, G. W. Kammlott, J. A. Herb, and C. F. Gardinier, Appl. Phys. Lett. **60**, 1576 (1992).

[10] J. E. Graebner, S. Jin, G. W. Kammlott, B. Bacon, L. Seibles, and W. Banholzer, J. Appl. Phys. **71**, 5353 (1992).

[11] J. E. Graebner, S. Jin, G. W. Kammlott, J. A. Herb, and C. F. Gardinier, Nature **359**, 401 (1992).

[12] J. E. Graebner, in *Proceedings of the Seventh International Conference on Phonon Scattering in Condensed Matter,* Ithaca,

NY, 1992, edited by M. Meissner and R. O. Pohl, Springer Series in Solid State Sciences Vol. 112 (Springer-Verlag, Berlin, 1993).
[13]D. G. Goodwin, J. Appl. Phys. **74**, 6888 (1993).
[14]D. G. Goodwin, J. Appl. Phys. **74**, 6895 (1993).
[15]J. E. Butler and R. L. Woodin, Philos. Trans. R. Soc. London **342**, 209 (1993).
[16]This effect has also been observed by J. A. Mucha and L. Seibles, in *Chemical Vapor Deposition of Refractory Metals and Ceramics II,* edited by T. M. Besmann, B. M. Gallois, and J. Warren, MRS Symposia Proceedings No. 250 (Materials Research Society, Pittsburgh, 1992), p. 357.
[17]D. F. Edwards and H. R. Philipp, in *Handbook of Optical Constants of Solids,* edited by E. D. Palik (Academic, Orlando, 1985), p. 655.
[18]G. S. Woods, J. A. Van Wyk, and A. T. Collins, Philos. Mag. B **62**, 589 (1990).
[19]G. S. Woods, G. C. Purser, A. S. S. Mtimkulu, and A. T. Collins, J. Chem. Phys. Solids **51**, 1191 (1990).
[20]J. Wilks and E. Wilks, *Properties and Applications of Diamond* (Butterworth-Heinemann, Oxford, 1991), p. 62.
[21]C. A. Klein, T. M. Hartnett, and C. J. Robinson, Phys. Rev. B **45**, 854 (1992).
[22]R. M. Chrenko, J. Appl. Phys. **63**, 5873 (1988).
[23]H. S. Carslaw and J. C. Jaeger, *Conduction of Heat in Solids,* 2nd ed. (Clarendon, Oxford, 1959), p. 139.
[24]W. J. Parker, R. J. Jenkins, C. P. Butler, and G. L. Abbott, J. Appl. Phys. **32**, 1679 (1961).
[25]A. C. Victor, J. Chem. Phys. **36**, 1903 (1962).
[26]R. Berman, *Thermal Conduction in Solids* (Oxford University, Oxford, 1976).
[27]T. R. Anthony, W. F. Banholzer, J. F. Fleischer, L. Wei, P. K. Kuo, R. L. Thomas, and R. W. Pryor, Phys. Rev. B **42**, 1104 (1990).
[28]D. G. Onn, A. Witek, Y. Z. Qiu, T. R. Anthony, and W. F. Banholzer, Phys. Rev. Lett. **68**, 2806 (1992).
[29]J. R. Olson, R. O. Pohl, J. W. Vandersande, A. Zoltan, T. R. Anthony, and W. F. Banholzer, Phys. Rev. B **47**, 14 850 (1993).
[30]L. Wei, P. K. Kuo, R. L. Thomas, T. R. Anthony, and W. F. Banholzer, Phys. Rev. Lett. **70**, 3764 (1993).
[31]V. I. Nepsha, V. R. Grinberg, Yu. A. Klyuev, and A. M. Naletov, Dokl. Akad. Nauk SSSR **317**, 96 (1991) [Sov. Phys. Dokl. **36**, 228 (1991)].
[32]R. Berman, Phys. Rev. B **45**, 5726 (1992).
[33]K. C. Hass, M. A. Tamor, T. R. Anthony, and W. F. Banholzer, Phys. Rev. B **45**, 7171 (1992).
[34]Y.-J. Han and P. G. Klemens, Phys. Rev. B **48**, 6033 (1993).
[35]J. Callaway, Phys. Rev. **113**, 1046 (1959).
[36]R. Berman and J. C. F. Brock, Proc. R. Soc. London A **289**, 46 (1965).
[37]P. G. Klemens, Proc. Phys. Soc. London Ser. A **68**, 1113 (1955).
[38]R. Berman, P. R. W. Hudson, and M. Martinez, J. Phys. C **8**, L430 (1975).
[39]L. A. Turk and P. G. Klemens, Phys. Rev. B **9**, 4422 (1974).
[40]C. A. Ratsifaritana and P. G. Klemens, Int. J. Thermophys. **8**, 737 (1987).
[41]J. W. Schwartz and C. T. Walker, Phys. Rev. **155**, 969 (1967).
[42]K. Neumaier, J. Low Temp. Phys. **1**, 77 (1969).
[43]R. Berman and M. Martinez, in *Diamond Research, 1976,* Suppl. to Ind. Diamond Rev., 7–13 (1976).
[44]V. I. Nepsha, V. R. Grinberg, Yu. A. Klyuev, N. A. Kolchemanov, and A. M. Naletov, Surf. Coatings Technol. **47**, 388 (1991).
[45]J. W. Schwartz and C. T. Walker, Phys. Rev. **155**, 959 (1967).
[46]H. B. G. Casimir, Physica **5**, 495 (1938).
[47]A. K. McCurdy, H. J. Maris, and C. Elbaum, Phys. Rev. B **2**, 4077 (1970).
[48]J. M. Ziman, *Electrons and Phonons* (Clarendon, Oxford, 1960).
[49]R. Berman, F. E. Simon, and J. M. Ziman, Proc. R. Soc. London Ser. A **220**, 171 (1953).
[50]R. Berman, E. L. Foster, and J. M. Ziman, Proc R. Soc. London Ser. A **231**, 130 (1955).
[51]D. R. Frankl and G. C. Campisi, in *Proceedings of the International Conference on Phonon Scattering in Solids, Paris, 1972,* edited by H. J. Albany (La Documentation Francaise, Paris, 1972), pp. 88–93.
[52]J. W. Vandersande, Phys. Rev. B **15**, 2355 (1977).
[53]V. I. Nepsha, N. F. Reshetnikov, Yu. A. Klyuev, G. B. Bokii, and Yu. A. Pavlov, Dokl. Akad. Nauk SSSR **283**, 374 (1985) [Sov. Phys. Dokl. **30**, 547 (1985)].
[54]The value of 0.53 used in Ref. 44 appears to be due to a confusion of diameter and radius of the sample. Perhaps it was meant to be the usual value of 1.12.
[55]P. G. Klemens has pointed out (private communication) that, in principle, a negative slope can arise from point-defect scattering and N processes in combination.
[56]D. T. Morelli, C. Uher, and C. J. Robinson, Appl. Phys. Lett. **62**, 1085 (1993).
[57]J. W. Vandersande, J. Phys. (Paris) Colloq. **39**, Suppl. **8**, C6-1017 (1978).
[58]R. E. Clausing, L. Heatherly, L. L. Horton, E. D. Specht, G. M. Begun, and Z. L. Wang, Diamond Relat. Mater. **1**, 411 (1992).
[59]A. V. Hetherington, C. J. H. Wort, and P. Southworth, J. Mater. Res. **5**, 1591 (1990).
[60]F. R. Sivazlian and B. R. Stoner (unpublished).
[61]L. H. Robins (private communication).
[62]J. E. Graebner, T. M. Hartnett, and R. P. Miller, Appl. Phys. Lett. **64**, 2549 (1994).
[63]For a review of thermal conductivity in CVD diamond, see, for example, J. E. Graebner, Diamond Films Technol. **3**, 77 (1993).

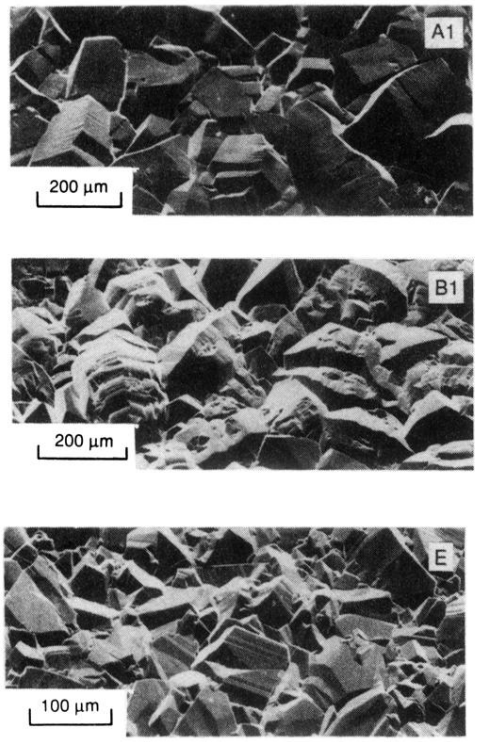

FIG. 1. Scanning-electron-microscope views of the top (growth) surfaces of microwave-plasma (MP) samples A1 and B1 and hot-filament (HF) sample E1. Note the relatively large and clean faces of samples A1 and E1, in contrast to the rough surfaces and secondary growth of sample B1. The smaller grain size of E1 is related to its thickness being $\sim\frac{1}{3}$ that of A1 or B1.

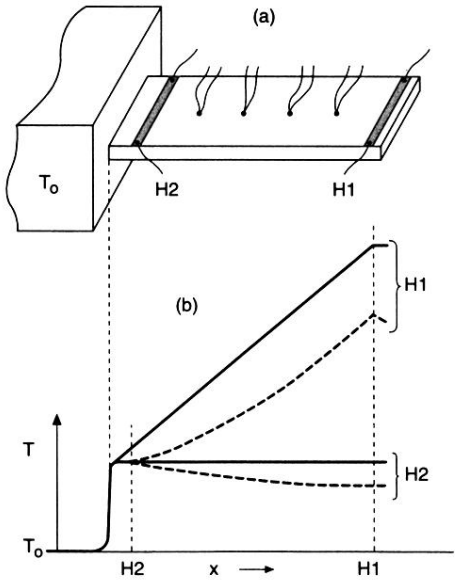

FIG. 3. (a) Schematic drawing of a sample mounted for measuring $\kappa_{\|}$. $H1$ and $H2$ are thin-film heaters deposited directly on the diamond sample, with four thermocouples (0.0025 cm diameter, Chromel-Constantan) attached with silver-filled epoxy. The sample is connected to a temperature-controlled (T_0) copper block with silver-filled epoxy. (b) Temperature distribution expected for electrical power applied to either $H1$ or $H2$, for two cases: zero radiation loss from the surface of the sample (solid straight lines) and severe radiation loss (dashed curves).